

## The structure behind it all

This article has been downloaded from IOPscience. Please scroll down to see the full text article.

2009 J. Phys.: Conf. Ser. 194 012001

(<http://iopscience.iop.org/1742-6596/194/1/012001>)

View [the table of contents for this issue](#), or go to the [journal homepage](#) for more

### Download details:

IP Address: 129.240.12.9

The article was downloaded on 31/01/2013 at 12:56

Please note that [terms and conditions apply](#).

# The Structure Behind it All

**Eva Lindroth, Luca Argenti, Jakob Bengtsson, Fabrizio Ferro,  
Michael Genkin, and Sølve Selstø<sup>1</sup>**

Atomic Physics, Fysikum, Stockholm University, AlbaNova University Center, SE-106 91  
Stockholm, Sweden

E-mail: [Eva.Lindroth@fysik.su.se](mailto:Eva.Lindroth@fysik.su.se)

**Abstract.** The talk discussed collisions where the structure of the systems involved plays a decisive role for the outcome of the event. For many types of charge changing processes the presence of resonant states can change the probability for a certain reaction by orders of magnitude. One example of this is electron-ion recombination where the resonant states are doubly or even multiply excited states lying above the ionization threshold of the recombined ion. The concept of a resonant state is discussed with the help of a simple model. The influence of such states is then illustrated through a few examples where some different calculational methods are compared with experiments. Finally, the possibility to also obtain accurate spectroscopical information from a collisional process is discussed.

## 1. Introduction

When photons, electrons or heavy particles collide with atomic systems, the probability for charge changing processes such as ionization or recombination is in many cases very sensitive to detailed structure of the systems. During the collisional process resonances may form which can provide an intermediate step between the initial and final state, hereby altering the probability for a process dramatically. An early example where this proved to be important was in the solar corona where Burgess showed [1] that the recombination of electrons with helium ions to atomic helium occurred mainly through resonances; so called dielectronic recombination dominated with two orders of magnitude over the non-resonant process of radiative recombination. This changed the expected ratio between ionization and recombination and explained why the corona temperature extracted from the ionization balance previously had been in disagreement with other methods to determine it.

Electron-ion recombination processes appear as important phenomena not only in the solar corona, but in many different types of plasma; astrophysical plasma in general [2], interstellar clouds [3], supernova reminiscence, and in connection with fusion [4]. The prediction of the atomic resonance structure is thus an important issue to understand and model these plasma. Unfortunately, the resonant structure varies significantly from element to element, and from charge state to charge state for the same element. This is especially true for resonances formed in low energy collisions where details in the structure determine if a resonance (above the ionization threshold) or a state (below the ionization threshold) is formed and this can easily alter the probability for recombination by an order of magnitude. Thus the detailed structure has a very strong impact on the probability for certain atomic processes.

<sup>1</sup> Present address: Center of Mathematics for Applications, University of Oslo, N-0316 Oslo, Norway

The interplay between structure and dynamics will be the subject of this article. We will use electron-ion recombination as our model process since the close relation is here very obvious, as will be discussed further in section 3, but of course similar scenarios can be found for other processes, e.g. for ionization, caused by photons or particles. Towards the end we give examples where it has been possible to go even further; not only is accurate structure needed to explain a dynamical process, but accurate studies of such a process can also give us structural information. However, we start in section 2 with a discussion of the very concept of a resonance.

## 2. Resonant states - a model example

To understand the concept of a resonant state it is illustrative to consider a very simple model potential that still can support resonances. Such a potential is the well formed by two  $\delta$  - function potential barriers separated by a distance, here  $2a$ ;

$$V(x) = \frac{\hbar^2 \alpha}{m} (\delta(x+a) + \delta(x-a)), \text{ with } \alpha > 0, a > 0, \quad (1)$$

where  $\alpha$  determines the potential strength. The resonances supported by this potential can be analyzed in several ways and the discussion below follows closely that outlined in Ref. [5]. A starting point can be to consider the solutions to the Schrödinger equation,  $H\Phi(x) = E\Phi(x)$ , with

$$H = -\frac{\hbar^2}{2m} \frac{\partial^2}{\partial x^2} + V(x). \quad (2)$$

These can be written down directly as

$$\begin{aligned} \Phi_I(x, E) &= Ae^{ikx} + Be^{-ikx}, \quad x < -a \\ \Phi_{II}(x, E) &= Ce^{ikx} + De^{-ikx}, \quad -a < x < a \\ \Phi_{III}(x, E) &= Fe^{ikx} + Ge^{-ikx}, \quad x > a, \end{aligned} \quad (3)$$

where  $E = \hbar^2 k^2 / 2m$ . We have here the classical text book scenario for potential scattering. The solutions in (3) have to be matched at  $x = \pm a$ , where the wave function must be continuous and its second derivative must have a singularity of the same degree as the delta-function. This means that the first derivative must have a singularity of the same degree as a Heaviside step-function. For  $x = -a$  this gives

$$-\frac{1}{2} \left( \left. \frac{\partial}{\partial x} \Phi_{II}(x) \right|_{-a} - \left. \frac{\partial}{\partial x} \Phi_I(x) \right|_{-a} \right) + \alpha \Phi_I(-a) = 0 \quad (4)$$

and a corresponding matching condition is obtained for  $x = a$ . These four matching conditions thus give four equations which can be solved to yield  $F$ ,  $B$ ,  $C$ , and  $D$  in (3), in terms of  $A$  and  $G$ :

$$F = \frac{1}{N} \left( Ak^2 + G(-2i\alpha)(k \cos(2ka) + \alpha \sin(2ka)) \right), \quad (5)$$

$$B = \frac{1}{N} \left( A(-2i\alpha)(k \cos(2ka) + \alpha \sin(2ka)) + Gk^2 \right), \quad (6)$$

$$C = \frac{1}{N} (A(k^2 + i\alpha k) + G(-i\alpha k e^{2ika})), \quad (7)$$

$$D = \frac{1}{N} (A(-i\alpha k e^{2ika}) + G(k^2 + i\alpha k)), \quad (8)$$

$$N = k^2 + 2ik\alpha - \alpha^2 + e^{4ika} \alpha^2. \quad (9)$$

In (5) and (6) we recognize the  $S$ -matrix, which relates incoming and outgoing waves:

$$\begin{pmatrix} B \\ F \end{pmatrix} = \begin{pmatrix} S_{11} & S_{12} \\ S_{21} & S_{22} \end{pmatrix} \begin{pmatrix} A \\ G \end{pmatrix}. \quad (10)$$

Assuming a situation where there is no incoming wave from the right, we can set  $G = 0$  and find the relative probabilities for reflection and transmission as

$$R = \left| \frac{B}{A} \right|_{G=0}^2 = |S_{11}|^2, \text{ and } T = \left| \frac{F}{A} \right|_{G=0}^2 = |S_{21}|^2. \quad (11)$$

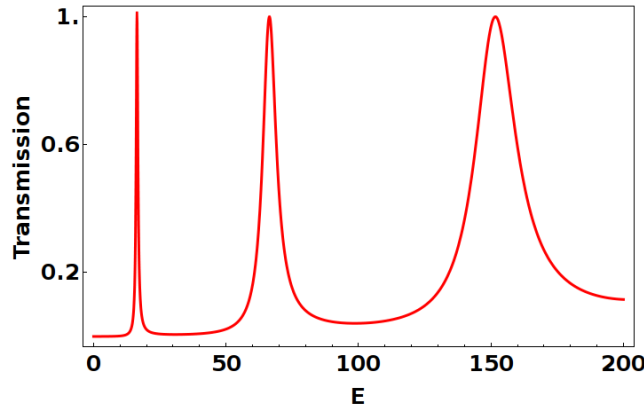


**Figure 1.** The transmission probability as a function of  $E = \hbar^2 k^2 / 2m$  of the incoming plane wave for  $\alpha = 20$  and  $a = 1/4$  for the model example discussed in section 2. All numbers are given in atomic units ( $m = \hbar = 1$ ).

In figure 1 the transmission probability for a particle is plotted as a function of the energy of the incoming wave for  $a = 1/4$  a.u. and  $\alpha = 20$ . The resonant behaviour is clearly seen. It is interesting to note that at the transmission peaks the probability reaches 100%, i.e. the potential is completely transparent for the incoming wave. If there was only one barrier there would always be reflection, but with two barriers the reflection vanishes for certain  $k$ . This can rather easily be concluded by inspection of (6) and is a, somewhat contra intuitive, effect of quantum interference. We note further that the amplitudes in (5 - 8) all have poles when the denominator,  $N$ , equals zero. Although there are no poles for real values of  $k$ , there is an infinite number of complex poles. For the parameters  $a = 1/4$  a.u. and  $\alpha = 20$ , as in figure 1, the first few are;

$$\begin{aligned} k_1 &= 5.72379 - 0.072053i, & k_2 &= 11.5103 - 0.266043i, & k_3 &= 17.3913 - 0.532731i, \dots \\ E_1 &= 16.3783 - 0.412416i, & E_2 &= 66.2082 - 3.062236i, & E_3 &= 151.087 - 9.264883i, \dots \end{aligned} \quad (12)$$

where  $k_i$ , and  $E_i$  are given in atomic units. These poles are closely related to the resonances observed in the transmission probability; in the vicinity of the  $i$ th pole the transmission coefficient can be approximated as

$$\frac{\text{Im}[E_i]^2}{(E - \text{Re}[E_i])^2 + \text{Im}[E_i]^2}. \quad (13)$$

Another way to find these poles is to solve ((3)) for both  $A = 0$  and  $G = 0$ , i.e to require that there are no incoming, but only outgoing waves. We will then find that (3) can only be satisfied for specific complex values of  $k$ , and these are precisely those which give  $N = 0$ . We can conclude that the observed resonant behaviour is a property of the potential itself, and it should not be necessary to solve the full scattering problem to understand it.

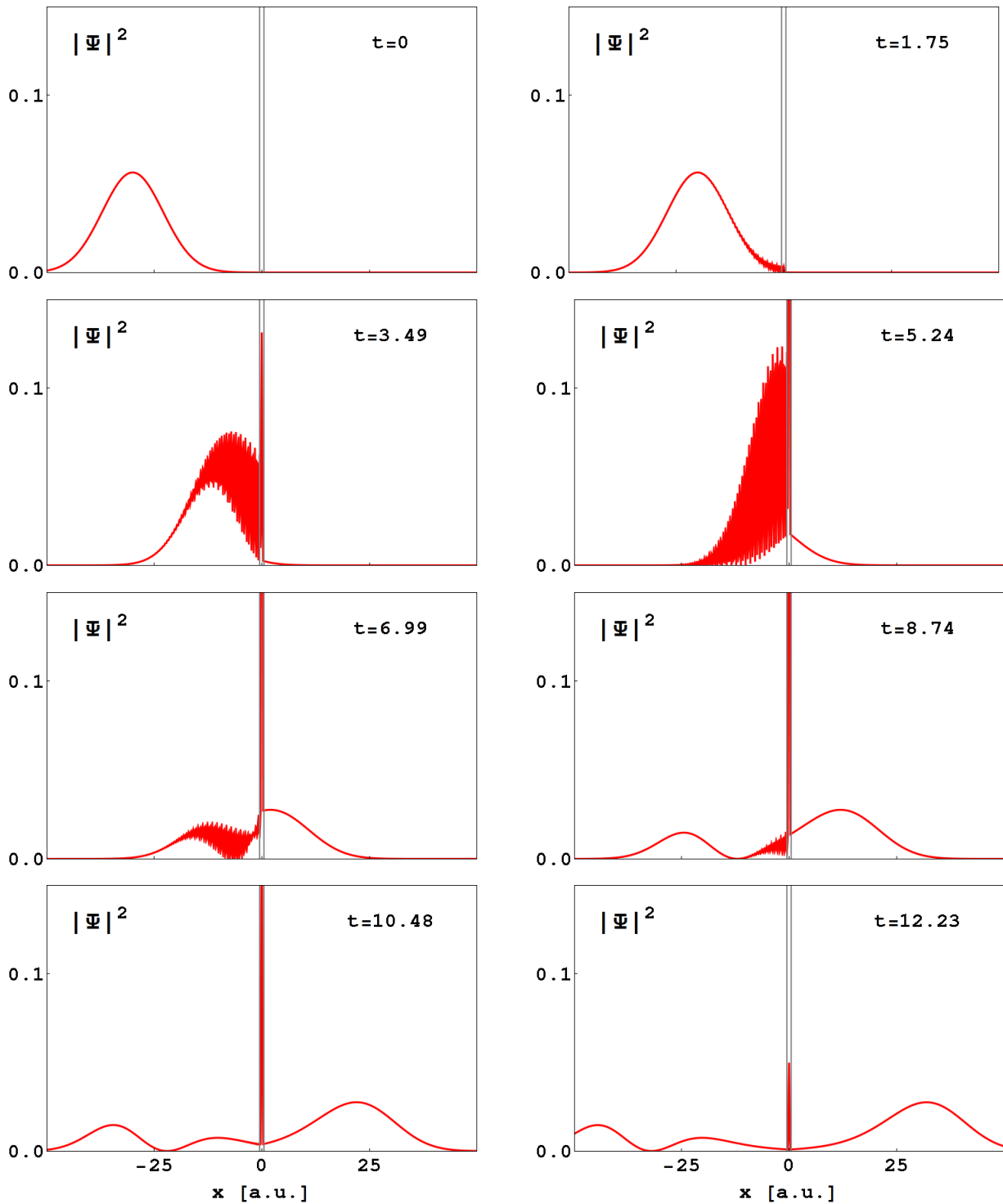


**Figure 2.** Snapshots showing how an electron, in the form of a wave packet, is scattered on a potential well constructed from two  $\delta$ -function potentials (indicated as thin gray lines). The red curves show the electron probability density.

We can get a more intuitive picture of the role of resonances if we consider a situation more similar to true electron scattering on the potential well. For this we simulate an incoming

electron with a wave packet and choose one with a wave number centered around the real part of the first pole ( $k_0 = \text{Re}[k_1]$  in(12)),

$$\phi(k) = \sqrt{\frac{2b}{\pi}} e^{-b(k-k_0)^2 - ikx_0}, \quad x_1 \ll -a, \quad k_1 > 0. \quad (14)$$

The wave packet is here centered around  $x_0$  in  $x$ -space. We make a Fourier transform to express the wave packet in  $x$ -space,

$$\psi(x, t = 0) = \frac{1}{\sqrt{2\pi}} \int_{-\infty}^{\infty} dk \phi(k) e^{ikx}. \quad (15)$$

The time propagation of the wave packet (with  $x_0 = -30$  and  $b = 50$ ) is shown as a few snapshots in figure 2. Each time-step corresponds to an interval within which a wave packet would travel the distance of ten length-units in the absence of any potential. The  $y$ -axis is kept constant to give a pedagogical picture of the time evolution. The strong peak that builds up inside the potential well actually reaches much higher than shown. For example at  $t = 6.99$  the peak reaches 1.4. The red areas are due to rapid oscillations of the wave function, caused by interference of the incoming and the reflected wave. It is clearly seen how the probability density builds up and then slowly leaks out from the potential well. This pronounced build-up only happens because the center of the incoming wave packet is *on resonance*. Note also that the time it takes for the wave packet to leak out is considerably longer than its translation time (the ten length-units per snap shot). To get a clearer picture of the decay from the well we plot the probability for the electron to be found inside it as a function of time, (figure 3). After a building-up phase the curve indicates a typical exponential decay rate which can be estimated to  $\lambda = 0.82$  per time unit (corresponding to a life-time of  $1/0.82$  a.u.). The decay rate is directly related to the *imaginary part* of the complex pole energy ( $-2 \text{Im}[E_1]/\hbar = 0.824\dots$ a.u.), indicating that the probability density inside the well can be described by a wave function decaying in time

$$\Psi(t) = \Psi(t_0) e^{-iE_i t} = \Psi(t_0) e^{-i\text{Re}[E_i]t} e^{\text{Im}[E_i]t} \implies |\Psi(t)|^2 = |\Psi(t_0)|^2 e^{2\text{Im}[E_i]t}, \quad (16)$$

where we note that  $\text{Im}[E_i] < 0$ .

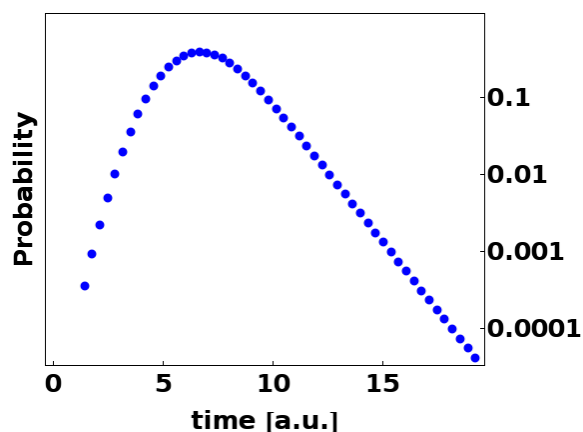


**Figure 3.** The probability for the electron to be found inside the potential well (cf. figure 2 ) as a function of time. For sufficiently long times the probability to find the electron inside the well decays exponentially.

A so called resonant state is not a state in the usual meaning. It is for example not normalizable, but the above example shows that it is characterized by strong localization. This is in contrast to a continuum state, but resembles the situation for a bound state. The resonant state has a well defined life-time due to the coupling to the continuum, and mathematically it

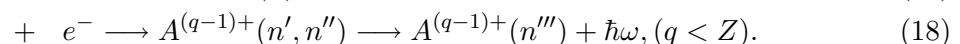
can be described as a complex pole of the  $S$ -matrix. With a long life-time, compared to e.g. the classical orbiting time, the resonance is “almost” bound and behaves as such a state, but there are also very short lived resonances whose life-time is of the same order of magnitude as the orbiting time. To understand the role resonances play in atomic processes the localization is very important. It provides a much better overlap with bound states than obtained with continuum electrons, increasing the probability of transitions. The long life-time also leads to a longer interaction time, compared to a non-resonant electron that just passes by. It is interesting to note that a *time-dependent* calculation of the process of dielectronic recombination of  $\text{He}^+$  [6] shows a situation very similar to that depicted in figure 2; when an incoming electron is on resonance a wave packet builds up in the vicinity of the nucleus, and it stays localized in this region for a time that is very long compared to that of a non-resonant electron with a nearby energy.

### 3. Recombination - when structure matters

As an example of a process where resonances are truly important we will now discuss electron-ion recombination. To start with we need a few basic facts about recombination.

#### 3.1. Dielectronic Recombination

The most fundamental process in the interaction of free electrons with ions is radiative recombination (RR). Here, process (17) below, the photon is directly emitted with the capture of an electron into the quantum state  $n$  of the ion  $A^{(q-1)}$ . This process can happen for any collision energy, i.e. it is *non-resonant*. In process (18), called dielectronic recombination (DR), a free electron is captured simultaneously with the excitation of a bound electron in the ion. Due to energy conservation, the binding of the captured electron plus its kinetic energy must equal the excitation energy of the bound electron, this is thus a process that can only happen when the incoming electron is on *resonance*. The resulting resonant (or doubly excited) state  $(n', n'')$  will generally have a very large probability to autoionize and loose the electron again, but it may emit a photon and end up in a state  $(n''')$  below the ionization threshold. This last step completes dielectronic recombination:



In (17 - 18)  $Z$  is the nuclear charge and  $q$  is the charge state. Both processes can be described as photo-recombination and can in principle provide two different pathways between the same initial and final states (i.e. when  $n = n'''$ ), thus there is a possibility of interference which would lead to asymmetric line profiles [7] in the recombination spectra. In reality such interference is seldom seen. There are several reasons for this. First, overlapping resonance profiles often mask the underlying asymmetry, and second, process (17) mainly populates the ground state, while process (18) mainly populates excited states, leading to very small asymmetries.

It is worth noting that the cross section for recombination scales as the inverse of the collisional energy, and thus goes to infinity when the electron energy goes to zero, which is another way of saying that the probability for recombination then goes to unity. The rate coefficients, i.e. the cross section times the electron velocity is, however, always finite. Still it is primarily the lowest energy region that can be dominated by recombination through process (17). The left panel of figure 4 shows a storage ring measurement [8, 9] (shaded area), of sodium-like silicon recombining into magnesium-like silicon. The peak at zero relative energy is due to radiative recombination. The rest of the spectrum is completely dominated by the resonant process of dielectronic recombination. The rate coefficient maps out the resonances of the ion which is

clearly seen when the experimental data are shown together with the level scheme of the doubly excited states as it is done in figure 4.

In storage rings cold electrons collide with cold ions and the recombination can be studied as function of the tunable relative energy, see Refs. [10, 11] for reviews. For plasma physics applications it is more common to show the rate coefficient as a function of temperature. In a plasma it is the finite energy distribution, given by the temperature, that can tune the electrons into resonance with the doubly excited states of the recombined ion. Rate coefficients displayed in this way are shown in the right panel of figure 4. Here, the blue line shows the storage ring results from the left panel (although for a wider energy range) folded with a Maxwellian energy distribution, see [8] for details, while the red curve shows a calculated prediction [12]. In Ref. [12] data for 22 sodium-like ions between  $\text{Mg}^+$  and  $\text{Xe}^{43+}$  were presented as a part of a larger effort to provide recombination data for all astrophysically relevant ions. Calculated data, obtained with the so called AUTOSTRUCTURE code, was then converted to a simple formula with fitting coefficients. We can see that the agreement is good for high temperatures. In this region the recombination rate is given by a large number of resonances where the exact position of each is not very crucial. For low temperatures (and thus mainly low collision energies) the situation is very different. Details in the treatment of the system like many-body effects, relativistic effects etc. are able to shift resonances below, closer to or further away from threshold, hereby dramatically changing the recombination rate prediction. This energy region is accordingly not at all as well represented with the data from the codes developed to efficiently address a large number of resonances and here we see a large discrepancy in figure 4.

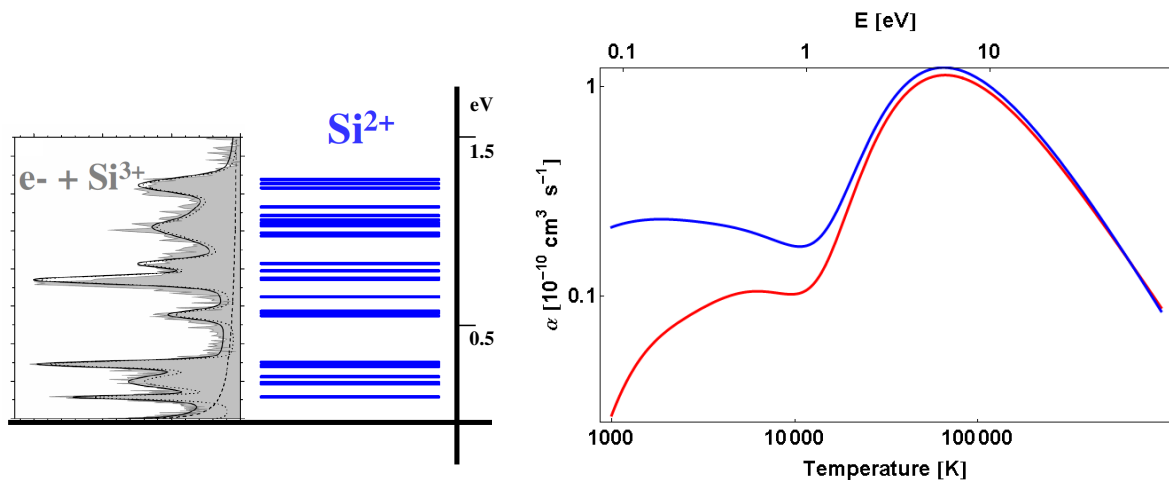


**Figure 4.** The left panel shows storage ring results [9] in the form of rate coefficients (shaded area) for  $\text{Si}^{3+}$  recombining into  $\text{Si}^{2+}$ . The thick line is the calculated cross section [9] folded with the electron beam temperature. The energies of the resonant states (doubly excited states) in  $\text{Si}^{2+}$  are shown in the form of a level scheme. It is obvious that the rate coefficients map out the energy level scheme. The right panel shows the rate coefficients as a function of temperature. The blue line shows the storage ring results folded with a Maxwellian energy distribution, see [8], while the red curve shows a theoretical prediction [12].

Now, sodium- and magnesium- like ions have in fact a rather simple electronic structure and hence it is possible to perform full many-body calculations for these systems. Such a calculation is of course more tedious and can in practice only be carried out for selected cases and selected energy ranges. The thick black line in figure 4 shows results from such a more dedicated effort with relativistic many-body perturbation theory (RMBPT) [9]. It is clear that it agrees well and

on an absolute scale with the experiment. Figure 5 shows more details from the calculation. For such low-charged systems as  $\text{Si}^{2+}$  and  $\text{Si}^{3+}$  it is the electron correlation that provides the largest obstacle for the calculation and from figure 5 it is evident that precise determination of many resonance positions is necessary for good agreement with experiment. A measure of the relativistic effects can be obtained from the broad peak around 0.2 eV. The three calculated peaks, slightly shifted compared to each other, are the three fine structure components of a resonance of  $^3\text{F}$ -symmetry. A more important relativistic effect is that several resonances are only coupled to the continuum due to spin-orbit coupling, i.e. without relativistic effects they would neither autoionize nor contribute to recombination. One example of this is the narrow peak at  $\sim 0.1$  eV.

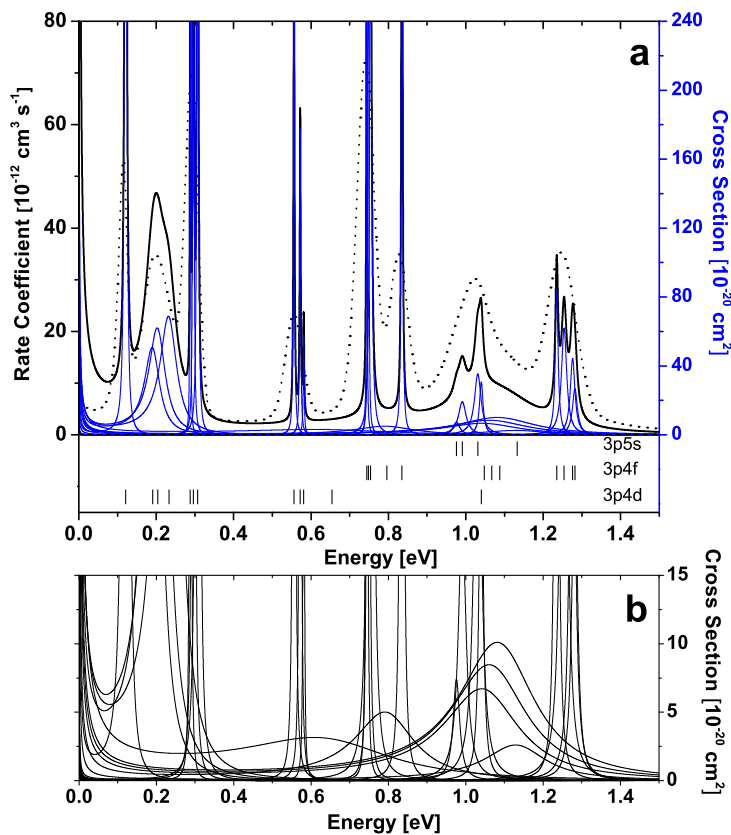


**Figure 5.** a. Individual cross sections of the low-energy DR resonances, obtained by the RMBPT calculation, are shown by thin solid lines (blue) with the corresponding electron configurations indicated by vertical bars. The thick solid line (black) shows the total DR cross section (sum of all individual DR resonances). Dots show the rate coefficients obtained from the convolution of the total DR cross section with the velocity distribution of the electrons from the experiment. b. shows a zoomed view of the individual DR cross sections, to emphasize the wide resonances.

An attempt on the same systems,  $\text{Si}^{3+}$  recombining into  $\text{Si}^{2+}$ , has been made also with another many-body method: multi-configurational Dirac-Fock (MCDHF) [13]. It is not very often that different theoretical approaches are compared systematically. When such a comparison has been made, see e.g. [14] for a comparison of MCDHF and RMBPT, it is usually found that they can produce as accurate results. Still the strong and weak points of the methods are slightly different. MCDHF is a versatile tool that can be applied to atoms and ions with more or less any shell structure, albeit a simple structure usually means better results. It also efficiently accounts for the bulk part of correlation among the valence electrons where a limited number of configurations dominate. Effects where many configurations contribute, but each with a tiny amount, as is the case for core-polarization, are more challenging. The strong point for MBPT is that it is very systematic. It is rather easy to know what has been included and where the approximations are made. For ions, and especially when the charge is increased, it benefits also from the fact that the more cumbersome higher-order contributions decrease in importance. For charged systems it is in addition usually quite easy to find a good enough starting point.

This is otherwise a weak point for perturbation theory and generally prevents its use on very correlated systems as e.g. resonances in negative ions. The MCDF calculation on dielectronic recombination of  $\text{Si}^{3+}$  [13] did not achieve the same detailed agreement with experiment as the preceding RMBPT-calculation and the main obstacle was the number of configurations that could be included in practice, underlying the fact that it is the problem to fully account for correlation which sets the accuracy for these systems.

There are of course other systems where a RMBPT- calculation simply could not be done, but where multi-configurational type calculations can do a very good job. Such an example is the recent study of recombination of  $\text{Ti}^{4+}$  ( $1s^2\dots 3p^6$ ) [15]. For low collision energies the dominating resonances in  $\text{Ti}^{3+}$  are due to  $1s^2\dots 3p^5 3dn\ell$  - resonances and the large number of LS-terms that can be formed from the  $3p^5 3d$  - configuration, each being the parent for a series of resonances, makes this a challenging problem. Still, in this forest of resonances, the most interesting finding in Ref. [15] is that two low lying resonances (below 1 eV and attributed to  $3p^5 3d^2 F$ ) change the recombination rate by two orders of magnitude in the low energy region, bringing theory in agreement with experiment [16]. This shows clearly what a careful treatment that is necessary to make reliable predictions of recombination rate coefficients. It is notable that the  $3p^5 3d^2 F$  resonances do not show up as distinct features in the experimental spectra. Both theory and experiment just show a flat spectrum in the sub-eV region, although enhanced with two orders of magnitude compared to the expected contribution from radiative recombination. Other many-body systems have shown the same behaviour [17, 18], only more pronounced. One of the most prominent example of this phenomena is the system of  $\text{Au}^{25+}$  [17]. The recombined ion  $\text{Au}^{24+}$  has the ground state configuration  $1s^2\dots 4p^6 4d^{10} 4f^9$ . In a series of papers Gribakin *et al* [19, 20, 21] have argued that the number of multiply excited states contributing to recombination in these systems is so large that statistical methods can be used. Distributing 19 active electrons (assuming a Kr-like inert core) among the orbitals  $4d_{3/2}$  to  $7g_{9/2}$ , they find 9000 configurations and  $10^8$  many-body states which potentially could contribute. This leads to a very high density of states just above the  $\text{Au}^{24+}$  ionization limit which can justify a statistical approach. Perhaps future development of such approaches will eventually result in methods that have predictive power also for complicated systems as  $\text{Au}^{24+}$ .

### 3.2. Complex rotation

Hitherto we have mainly discussed the resonant states contributing to recombination as doubly or multiply excited states and not really considered their true nature as resonances. As discussed in section 2 some resonances are so narrow that they really do appear as more or less bound states. They can still contribute to recombination since the recombination strength is mainly given by the ratio  $S \sim (A_a A_r)/(A_a + A_r)$  where  $A_a$  is the recombination rate into the resonance (which is equal to its autoionization rate for resonances above the first, but not the second, ionization limit), and  $A_r$  is the radiative rate to a bound state. Usually the radiative rate is much slower than the autoionization rate and the latter can thus vary over many orders of magnitude before it makes any difference to the recombination. It is therefore often possible to calculate the doubly excited states with the autoionization channel turned off and than just consider it to lowest order. In short that is the method of the MCDF calculation [13] discussed above. To go beyond that approach one possibility is to do a full scattering calculation, a widely used method here is the R-MATRIX method, see e.g. [22, 23, 24]. Comparing with the discussion in section 2 a full scattering calculation implies to consider both the incoming and the outgoing wave to the interaction region. Another possibility is to consider just the outgoing wave. For the atom this means that we consider a doubly excited state, without considering the population of it, and allow it to decay by emitting an electron. One way to do that is to use the method of complex rotation [25, 26] (or complex scaling), which since the seventies has developed into a widely spread tool to handle resonances in atoms and molecules, see e.g.

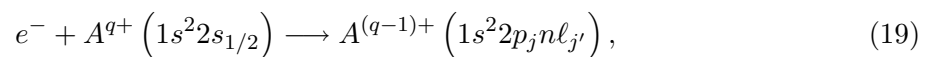
the discussion and references in Ref. [27]. The radial coordinate is then scaled with a complex constant,  $r \rightarrow re^{i\theta}$ . Mathematically complex scaling prevents the representation of any incoming electron, but allows a good representation of the outgoing wave. As in the model example in section 2, the resonances will now appear as discrete states with complex energies, where the half width due to autoionization will be given by the imaginary part of the energy. The decay of a quantum system is a form of dissipation and complex scaling can be shown to be closely related to other methods to describe dissipation [28].

Since dielectronic recombination (18) is a form of photo-recombination we can use detailed balance and obtain the recombination cross section through a certain resonance as the time inverse of photoabsorption to it, which with complex rotation is conveniently calculated as the imaginary part of the polarizability, see Ref. [29] for details. In this way the recombination cross section can be obtained directly from the resonance and its coupling to the continuum (Auger width) as well as to the bound states (radiative width) without any explicit account for the full scattering event. In this context it is again interesting to study the broad peak around 0.2 eV in figure 5. Although the width of most peaks in the experimental spectrum is given by the electron beam temperature, this peak has a broad internal width which is clearly resolved by the experiment (figure 4), and which is accurately mapped out by the calculation. Over the last decade the combination of many-body perturbation theory and complex rotation has been used to determine recombination cross sections for a number of elements and charge states, primarily in lithium-like systems [30, 31, 32, 33, 29, 34, 35, 36, 37], but also a few other one-valence ions have been considered [38, 18, 39, 40, 9].

#### 4. Collisions for Spectroscopy

Finally, we would like to mention the development of dielectronic recombination studies into a new spectroscopical tool. An early example where such resonances were used to accurately determine an excitation energy in a highly charged ion was the  $4p_{1/2} - 4s$  splitting in copper-like lead [18] which was determined with an accuracy of  $\sim 1$  meV, corresponding to a precision of  $8 \times 10^{-6}$ . During later years it has been possible to study hyperfine structure and isotope shifts through dielectronic recombination resonances [40, 37, 41]. In Ref. [37] the  $2s_{1/2} - 2p_{3/2}$  transition energy in lithium-like scandium was determined with an accuracy of 4.6 ppm. Hereby the evaluation of radiative contributions such as self energy and vacuum polarization in a many electron environment can be put to a stringent test as discussed in Ref. [37]. We will discuss the method with this system as the example.

The method is based on the nearly complete cancellation between the target excitation energy and the binding energy of the attached electron for certain low energy resonances. For a lithium-like system a resonance can be formed in the following way;



where  $E(1s^2 2p_j n l_{j'}) > E(1s^2 2s_{1/2})$ . For a highly charged system the state  $n l_{j'}$  will be a Rydberg state; for lithium-like  $\text{Sc}^{18+}$  the lowest resonances are e.g. found for  $n = 10$  and for  $\text{Kr}^{33+}$  for  $n = 15$ . The resonance will be found at energies

$$\varepsilon = E(1s^2 2p_j) - E(1s^2 2s) - \Delta E, \quad (20)$$

where  $\Delta E$  is the binding energy of the outer Rydberg electron. This binding energy can be accurately determined by calculations since it is dominated by the Dirac energy and only small corrections are given by many-body effects. With  $Z = 18$ , the Dirac hydrogen-like binding energy is 44.114 29 eV for  $10d_{3/2}$  and 44.101 57 eV for  $10d_{5/2}$ . This value is thus obtained under the assumption that the core screens exactly three units of charge. If we include the interaction

with the inner  $1s^2$  core through the Dirac-Fock potential we obtain instead 44.21387 eV and 44.20009 eV respectively, and adding also the Breit interaction and true correlation effects from the  $1s^2$  core we get a further, but slight, change to 44.21458 eV and 44.20093 eV. It remains now to add the interaction with the  $2p$ -electron. This interaction is term-dependent and we see in table 1 the results for the three lowest resonances  $(2p_{3/2}10d_{3/2})_{J=2}$ ,  $(2p_{3/2}10d_{3/2})_{J=3}$  and  $(2p_{3/2}10d_{5/2})_{J=4}$ . The first line, labeled first order Coulomb interaction, gives the results after diagonalization of the Hamiltonian matrix of all  $2p_j10\ell_j$  configurations, coupled to one specific  $J$ . In particular this means that  $(2p_{3/2}10d_{3/2})_J$  and  $(2p_{3/2}10d_{5/2})_J$  are allowed to mix. We see in table 1 that the results for the three terms are now changed by up to 70 meV compared to the situation before adding the detailed interaction with the  $2p$ -electron. After inspection of the other entries in table 1 we can conclude that only two types of contributions, namely from the core Dirac-Fock potential discussed above and from the first order Coulomb matrix element, are in the 10 meV range. These effects are well defined and can be unambiguously calculated. At the next level contributions of a few meV are coming from true electron correlation, while additional interactions and higher order effects give even smaller contributions. It is the smallness of all these contributions that gives the high accuracy with which the binding energy can be calculated for a Rydberg electron. The errors given for the calculated values in table 1 represent neglected contributions from high partial-wave angular momenta ( $\ell = 12 - \infty$ ) contributions to the second order correlation energy as well as uncalculated higher-order correlation, conservatively estimated from the calculated all-order ladder diagram. Now these calculated Rydberg electron binding energies can be combined with the measured resonance positions [37] to extract the target excitation energy. Since we have results for three resonances it can be done in three different ways. The results are shown in table 1. The three resonances provide slightly different results for the  $2p_{3/2} - 2s_{1/2}$  energy splitting, but the differences are within the estimated error bars confirming the expected accuracy of the method.

**Table 1.** Term energies for the lowest lying  $\text{Sc}^{17+}(1s^22p_{3/2}10d_j)_J$  resonances. Results in eV.

	J=2	J=3	J=4
Coulomb interaction 1st order	-44.27255	-44.23494	-44.27570
Breit interaction 1st order	0.00063	- 0.00002	- 0.00013
mass polarization 1st order	- 0.00002	- 0.00001	- 0.00005
Coulomb int. 2nd order (ladder diag.)	- 0.00288	- 0.00574	- 0.00383
Breit -Coulomb 2nd order (ladder diag.)	0.00000	- 0.00002	0.00000
higher- order Coulomb correlation	- 0.00008	- 0.00001	0.00011
core polarization of $2p_{3/2}10d_j$ interaction	0.00011	0.00004	0.00044
Total	-44.27480 (11)	-44.24071 (9)	-44.27916 (11)
Exp [37]	0.03465 (10)	0.06861 (10)	0.03036 (10)
Extracted energy: $2s_{1/2} - 2p_{3/2}$	-44.30945 (15)	-44.30932 (15)	-44.30952 (15)

#### 4.1. The effect of hyperfine structure on the recombination resonances

If the nucleus of the considered ion has spin the doubly excited states will split due hyperfine structure and with high enough experimental resolution this can be seen in the recombination rate coefficients, as in the measurement on lithium-like scandium in Ref. [37]. How will the cross section change and how can we account for it? Since the interaction with the nuclear magnetic

moment scales with the principal quantum number as  $1/n^3$ , we can usually neglect it for a Rydberg state and thus the hyperfine splitting is given by the interaction of the nuclear spin,  $I$ , with the inner electrons. The dominating contribution will be with the unpaired electron, for lithium-like scandium that is with the  $n = 2$  electron. How will that affect a resonance of the form  $(2p j_{low} n \ell j_{high})_J$ ? To analyze this it is convenient to express the coupling of the total *electron* angular momenta,  $J$ , with the *nuclear* angular momenta,  $I$ , to a grand total angular momenta  $K$  in terms of a different coupling scheme where we first couple the nuclear spin,  $I$ , to the electron angular momentum of the target ion to form  $F$ , and then  $F$  to the angular momentum of the outer electron to form  $K$ . These two coupling schemes are related as:

$$\begin{aligned} & | \{ I (j_{low} j_{high}) J \} K_{tot} \rangle = \sum_F c_F | \{ (I j_{low}) F j_{high} \} K_{tot} \rangle \\ & = \sum_F (-1)^{j_{low} + j_{high} + I + K_{tot}} \sqrt{(2F + 1)(2J + 1)} \begin{Bmatrix} K_{tot} & F & j_{high} \\ j_{low} & J & I \end{Bmatrix} | \{ (I j_{low}) F j_{high} \} K_{tot} \rangle. \end{aligned} \quad (21)$$

Knowing the hyperfine splitting of the states in the target ion we can now directly calculate the hyperfine splitting of the doubly excited states which (depending on the nuclear spin) can split in up to  $2K + 1$  states.

A lithium-like target ion ground state ( $1s^2 2s_{1/2}$ ) splits into two levels which in an experiment can be statistically populated. In Ref. [37] this splitting was experimentally resolved. From each of these,  $2K + 1$  resonances can (generally) be populated, resulting in two groups, each containing  $2K + 1$  resonances, where we previously just had one recombination resonance. The individual members in the groups could not be resolved in Ref. [37], but their positions and strengths still affected the line shape and had to be accounted for in the data analysis. The strength of a resonance ( $K$ ) populated *from* a particular state  $F$  of the target ion is given by:

$$S(F, K) = \frac{g_K}{g_F} \frac{A^r(K) A_F^a(K)}{A^r(K) + A^a(K)}, \quad (22)$$

where  $A_F^a(K)$  is the *partial* autoionization rate to the ion state  $F$  and  $A^a(K) = \sum_F A_F^a(K)$ . The multiplicities of the levels with angular momentum  $F$  and  $K$  are given by  $g_K$  and  $g_F$ , and  $A^r(K)$  is the stabilizing radiative rate from the doubly excited state to any bound state. Since  $J$  is approximately a good quantum number (the term splitting is much larger than the hyperfine-structure splitting) it should be justified to assume that  $A^a(K)$  to a good approximation is unaffected by the presence of the hyperfine interaction and can be set to  $A^a(K) = A^a(J)$ , but this is not enough since in (22) we really need the partial width to each  $F$ . For this purpose we can relate (22) to the recombination strength without hyperfine interaction. The latter strength is proportional to the autoionization rate from state  $J$ , which is a sum of contributions from several channels for autoionization ( $2s\epsilon\ell j'_{high}$ ) and we can write

$$S(J) = \sum_{j'_{high}} \frac{g_J}{g_{j_{low}}} \frac{A^r(J) A^a(J, j'_{high})}{A^r(J) + A^a(J)}. \quad (23)$$

where  $A^a(J, j'_{high})$  is the *partial* autoionization rate to the  $2s\epsilon\ell j'_{high}$ -continuum from state  $J$ . Now the nuclear spin can be coupled to this continuum in the same way as it was done in (21), but now with the  $2s_{1/2}$  electron as the one with angular momentum  $j_{low}$  and  $j'_{high}$  as the angular momentum of the autoionized electron. We will then find  $A_F^a(K, j'_{high})$  as a sum over rates  $A^a(J, j'_{high})$ :

$$S(F, K) = \sum_{j'_{high}} \frac{g_K}{g_F} \frac{A^r(K) A_{F, j'_{high}}^a(K)}{A^r(K) + A^a(K)} = \sum_{j'_{high}} \frac{g_K}{g_F} \frac{A^r(K) A^a(J, j'_{high})}{A^r(K) + A^a(J)} \begin{Bmatrix} K_{tot} & F & j'_{high} \\ j_{low} & J & I \end{Bmatrix}^2. \quad (24)$$

In general the autoionization widths to the different hyperfine levels of the target are truly different. Since different continua ( $2s_{1/2}\varepsilon\ell j'_{high}$ ) are more or less important for the decay of different doubly excited states  $2p_{3/2}n\ell j_{high}$ , this is directly transferred to a preference for decay to certain  $F$ . This is an effect of angular momentum coupling and does not depend on the size of the hyperfine splitting, but without any hyperfine splitting the decay to different  $F$  can of course not be distinguished.

The example of  $\text{Sc}^{18+}$  has highlighted the fact that dielectronic recombination can be used as an accurate spectroscopical tool. For heavy [41], and perhaps even radioactive, nuclei this development has opened a new path to accurate information concerning nuclear properties. Although measurements on hyperfine structure and isotope shifts have been used for this purpose during many decades, the method has always been hampered by the limitations of the atomic theory necessary to extract the nuclear information. The use of highly charged ions, where a suitable electron configuration can be freely chosen, changes this dramatically.

## 5. Conclusions

We have discussed some aspects of the role played by structure in collisions, both with respect to our ability to make good enough predictions for applications and with respect to new perspectives for spectroscopy.

## Acknowledgments

The authors thank the colleagues responsible for the experimental studies discussed in this talk; A. Müller, S. Schippers, R. Schuch, A. Wolf and their co-workers for all their contributions during many years of collaboration. Financial support from the Swedish Science Research Council (VR) and from the Göran Gustafsson Foundation is gratefully acknowledged. The expressions for resonance strengths when the hyperfine structure is resolved have been obtained in collaboration with A. Wolf.

## References

- [1] Burgess A 1964 *Astrophys. J.* **139** 776
- [2] Dubau J and Volonte S 1980 *Reports on Progress in Physics* **43** 199
- [3] Osterbrock D E 1989 (Mill Valley, California: Univ. Science Books)
- [4] Hahn Y 1995 *Atomic and Molecular Processes in Fusion Edge Plasmas* ed Janev R (New York: Plenum Publ. Corp.) p 91
- [5] Brandefelt N Thesis, Stockholm University 2001
- [6] Mitnik D M, Griffin D C and Pindzola M S 2002 *Phys. Rev. Lett.* **88** 173004
- [7] Fano U 1961 *Phys. Rev.* **124** 1866
- [8] Orban I, Glans P, Altun Z, Lindroth E, Källberg A and Schuch R 2006 *A&A* **459** 291–296
- [9] Orban I, Lindroth E, Glans P and Schuch R 2007 *J. Phys. B* **40** 1063
- [10] Schuch R and Böhm S 2007 *Journal of Physics: Conference Series* **88** 012002
- [11] Müller A 2009 *Journal of Physics: Conference Series* **xx** xx
- [12] Altun Z, Yumak A, Badnell N R, Loch S D and Pindzola M S 2006 *A&A* **447** 1165–1174
- [13] Schmidt E W, Bernhardt D, Müller A, Schippers S, Fritzsche S, Hoffmann J, Jaroshevich A S, Krantz C, Lestinsky M, Orlov D A, Wolf A, Lukić D and Savin D W 2007 *Physical Review A* **76** 032717
- [14] Rodrigues G C, Ourdane M A, Bierón J, P Indelicato and Lindroth E 2001 *Phys. Rev. A* **63** xx
- [15] Nikolić D, Gorczyca T W and Badnell N R 2009 *Phys. Rev. A* **79** 012703
- [16] Schippers S, Bartsch T, Brandau C, Gwinner G, Linkemann J, Müller A, Saghiri A A and Wolf A 1998 *Journal of Physics B: Atomic, Molecular and Optical Physics* **31** 4873–4886
- [17] Hoffknecht A, Uwira O, Frank A, Haselbauer J, Spies W, Angert N, Mokler P H, Becker R, Kleinod M, Schippers S and Müller A 1998 *J. Phys. B* **31** 2415–2428
- [18] Lindroth E, Danared H, Glans P, Pešić Z, Tokman M, Viktor G and Schuch R 2001 *Phys. Rev. Lett.* **86** 5027
- [19] Gribakin G F, Gribakina A A and Flambaum V V 1999 *Aust. J. Phys.* **52** 443
- [20] Flambaum V V, Gribakina A, Gribakin G F and Harabati C 2002 *Phys. Rev. A* **66** 012713
- [21] Gribakin G F and Sahoo S 2003 *J. Phys. B* **36** 3349
- [22] Burke P G, Hibbert A and Robb W D 1971 *J. Phys. B* **4** 153–161

- [23] Nahar S N and Pradhan A K 1992 *Phys. Rev. Lett.* **68** 1488–1491
- [24] Robicheaux F, Gorczyca T W, Pindzola M S and Badnell N R 1995 *Phys. Rev. A* **52** 1319–1333
- [25] Balslev E and Combs J 1971 *Commun. Math. Phys.* **22** 296
- [26] Simon B 1972 *Commun. Math. Phys.* **27** 1
- [27] Bengtsson J, Lindroth E and Selstø S 2008 *Physical Review A* **78** 032502
- [28] Genkin M and Lindroth E 2008 *J. Phys. A* **41** 425303
- [29] Tokman M, Eklöv N, Glans P, Lindroth E, Schuch R, Gwinner G, Schwalm D, Wolf A, Hoffknecht A, Müller A and Schippers S 2002 *Phys. Rev. A* **66** 012703
- [30] Zong W, Schuch R, Lindroth E, Gao H, DeWitt D R, Asp S and Danared H 1997 *Phys. Rev. A* **56** 386
- [31] Mannervik S, DeWitt D, Engström L, Lidberg J, Lindroth E, Schuch R and Zong W 1998 *Phys. Rev. Lett.* **81** 313–316
- [32] Glans P, Lindroth E, Badnell N R, Eklöv N, Zong W, Justiniano E and Schuch R 2001 *Phys. Rev. A* **64** 043609
- [33] Madzunkov S, Lindroth E, Eklöv N, Tokman M, Paál A and Schuch R 2002 *Phys. Rev. A* **65** 032505
- [34] Mohamed T, Nikolić D, Lindroth E, Madzunkov S, Fogle M, Tokman M and Schuch R 2002 *Phys. Rev. A* **66** 022719
- [35] Nikolic D, Lindroth E, Kieslich S, C Brandau S S, Shi W, Müller A, G Gwinner M S and Wolf A 2004 *Phys. Rev. A* **70** 062723
- [36] Kieslich S, Schippers S, Shi W, Müller A, Gwinner G, Schnell M, Wolf A, Lindroth E and Tokman M 2004 *Phys. Rev. A* **70** 042714
- [37] Lestinsky M, Lindroth E, Orlov D A, Schmidt E W, Schippers S, Böhm S, Brandau C, Sprenger F, Terekhov A S, Müller A and Wolf A 2008 *Phys. Rev. Lett.* **100** 033001
- [38] DeWitt D R, Lindroth E, Schuch R, Gao H, Quinteros T and Zong W 1995 *J. Phys. B* **28** L147–L153
- [39] Fogle M, Eklöv N, Lindroth E, Mohamed T, Schuch R and Tokman M 2003 *J. Phys. B* **36** 2563
- [40] Schuch R, Lindroth E, Madzunkov S, Fogle M, Mohamed T and Indelicato P 2005 *Phys. Rev. Lett.* **95** 183003
- [41] Brandau C, Kozhuharov C, Harman Z, Muller A, Schippers S, Kozhedub Y S, Bernhardt D, Bohm S, Jacobi J, Schmidt E W, Mokler P H, Bosch F, Kluge H J, Stohlker T, Beckert K, Beller P, Nolden F, Steck M, Gumberidze A, Reuschl R, Spillmann U, Currell F J, Tupitsyn I I, Shabaev V M, Jentschura U D, Keitel C H, Wolf A and Stachura Z 2008 *Phys. Rev. Lett.* **100** 073201